INORGANIC CHEMISTRY FRONTIERS

CCS 中国化学会 CHINESE CHEMICAL SOCIETY

ROYAL SOCIETY OF CHEMISTRY

Improved Deep-Red Phosphorescence in Cyclometalated Iridium Complexes via Ancillary Ligand Modification

Journal:	*Inorganic Chemistry Frontiers*
Manuscript ID	QI-RES-12-2019-001584.R2
Article Type:	Research Article
Date Submitted by the Author:	01-Feb-2020
Complete List of Authors:	Kabir, Evanta; University of Houston Wu, Yanyu; University of Houston Sittel, Steven; University of Houston Nguyen, Boi-Lien; University of Houston Teets, Thomas; University of Houston

ARTICLE

Improved Deep-Red Phosphorescence in Cyclometalated Iridium Complexes via Ancillary Ligand Modification

Received 00th January 20xx,
Accepted 00th January 20xx

DOI: 10.1039/x0xx00000x

Evanta Kabir, Yanyu Wu, Steven Sittel, Boi-Lien Nguyen, and Thomas S. Teets*[a]

In this work, we describe bis-cyclometalated iridium complexes with efficient deep-red luminescence. Two different cyclometalating (C^N) ligands–1-phenylisoquinoline (piq) and 2-(2-pyridyl)benzothiophene (btp)–are used with five strong π-donating ancillary ligands (L^X) to furnish a suite of nine new complexes with the general formula $Ir(C^N)_2(L^X)$. Improvements in deep-red photoluminescence quantum yields were accomplished by the incorporation of sterically encumbering substituents onto the ancillary ligand, which can enhance the radiative rate constant (k_r) and/or reduce the non-radiative rate constant (k_{nr}). Five of the complexes were characterized by X-ray crystallography, and all of them were investigated by in-depth spectroscopic and electrochemical measurements.

Introduction

Luminescent cyclometalated iridium(III) complexes have become one of the most prominent classes of molecular phosphors, contributing to numerous applications in photocatalysis,[1–3] bioimaging, and sensing,[4,5] and most notably, organic light-emitting diodes (OLEDs)[6–9] and light-emitting electrochemical cells.[10,11] These compounds luminesce from triplet excited states with ligand-centered (^{3}LC or $^3\pi\pi^*$) and metal-to-ligand charge transfer (^{3}MLCT or $^3d\pi^*$) character, mixing through configuration interaction. Homoleptic complexes of the type *fac*-$Ir(C^N)_3$ (C^N = cyclometalating ligand) are popular in both OLED and photocatalysis applications,[1,12,13] and heteroleptic complexes of type $Ir(C^N)_2(L^X)$ (L^X = ancillary ligand) have also become prominent. The ancillary ligands in the heteroleptic complexes can strongly influence the emission color,[14,15] but most often shift redox potentials (especially the formally Ir^{IV}/Ir^{III} couple) and perturb the excited state dynamics, while only subtly influencing the photoluminescence spectrum.[16,17]

Facile color tunability, high photoluminescence quantum yields (Φ_{PL}), and relatively short phosphorescence lifetimes (τ) are some of the key features of cyclometalated iridium(III) complexes, which along with their good thermal and photostability lead to applications in diverse fields. There are many examples of iridium(III) complexes which emit in the blue to orange regions of the spectrum with near unity quantum yields,[18–22] but red and near-infrared emitters in the lower-energy regions of the spectrum typically have lower quantum yields, which is an important performance metric to function in commercial devices. Given their widespread success in optoelectronics, most recent developments in deep-red and near-infrared (NIR) phosphorescence have focused on cyclometalated iridium complexes, although there have been successes with complexes of several other transition metals as well.[23,24] As representative examples, complexes of rhenium,[25,26] ruthenium,[27,28] osmium,[29,30] and platinum[31–38] have all been designed to phosphoresce with moderate to excellent quantum yields in the low-energy regions of the visible spectrum and beyond, with some of these complexes showing promise in OLED applications. Select platinum complexes have some of the most impressive deep-red/NIR phosphorescence efficiencies outside of iridium, and while many platinum phosphors emit out of aggregated states and thus require high concentrations to exhibit deep-red or NIR luminescence,[34,36,38] a recent diplatinum design was successful at engendering red emission with high quantum yields sans aggregation.[37]

The challenge in designing efficient deep-red to NIR molecular phosphors is twofold. The photoluminescence quantum yield (Φ_{PL}), defined as the ratio of emitted photons to absorbed photons, can also be expressed as the ratio of the radiative rate constant (k_r) to the sum of radiative and non-radiative (k_{nr}) rate constants. According to the energy gap law,[39,40] the non-radiative rate constant (k_{nr}) increases for complexes with lower-energy excited states, on account of greater vibrational overlap between the ground and excited states.[41] On the other hand, the radiative rate (k_r) has a cubic dependence on the transition energy and is expected to be smaller when longer emission wavelengths are accessed.[6] The radiative rate constant k_r has a strong dependence on the spin-orbit coupling (SOC) in the excited state, which derives exclusively from the MLCT states that contribute to the emissive triplet state, T_1. The excited-state MLCT character is sensitive to the nature of the ancillary ligand in heteroleptic bis-cyclometalated iridium complexes, so synthetic strategies

[a] *Department of Chemistry, University of Houston, Lamar Fleming Jr. Building, 3585 Cullen Blvd. Room 112, Houston, TX 77204-5003*
**E-mail: tteets@uh.edu*

Electronic Supplementary Information (ESI) available: X-ray crystallographic summary tables, additional X-ray crystal structures, additional cyclic voltammograms, UV-vis absorption and excitation spectra, 77-K emission spectra, and NMR spectra of new complexes. See DOI: 10.1039/x0xx00000x

which augment the MLCT character can lead to increases in k_r and improvements in Φ_{PL}.

Using the above insights, our group has made significant advances in the performance of cyclometalated iridium complexes which emit in the low-energy regions of the visible spectrum. Our strategy involves the incorporation of nitrogen-donor, electron-rich ancillary ligands into heteroleptic $Ir(C^N)_2(L^X)$ complexes. We have shown that this strategy can lead to significant improvements in the photoluminescence quantum yields of yellow-orange[17] and red-emitting[42] compounds, with quantum yields as high as 0.8 for the red emitters. Subsequent work on related compounds revealed additional structure-property relationships in these red-emitting compounds, showing how the ancillary ligand structure (chelate ring-size, donor atoms, and substituents) influenced the nature of the excited state and the excited-state dynamics.[43] One finding from these studies is that when the cyclometalated aryl group is a simple phenyl ring, as is the case for red-emitting compounds where C^N = 1-phenylisoquinoline (piq), the photoluminescence wavelength is very sensitive to the electron-richness of the ancillary ligand, leading to deep-red luminescence (defined here as $\lambda_{max} > 650$ nm) for some ancillary ligands. For example, the complex $Ir(piq)_2(dipba)$ (dipba = *N,N*-diisopropylbenzamidinate) has a photoluminescence λ_{max} of 671 nm in room-temperature THF solution, with a respectable quantum yield of 0.34.[42,43] That said, the two deep-red emitters we prepared in these previous works had k_r values that were smaller and, particularly evident, k_{nr} values that were larger than the structurally related compounds that phosphoresce in the red region, limiting their quantum yields to fairly modest values. Further improvements in the quantum yields require synthetic strategies capable of augmenting the k_r values and/or decreasing the k_{nr} values for compounds which emit in the deep red portion of the spectrum.

In this work we present synthetic modifications that lead to improved deep-red-emitting cyclometalated iridium complexes. Two key findings of this report are (i) sterically encumbering substituents on the electron-rich ancillary ligand can lead to significant improvements in Φ_{PL} for deep-red phosphors, and (ii) making the ancillary ligand even more electron rich can shift the photoluminescence to the near-infrared (NIR) region, $\lambda_{max} > 700$ nm. Our work here describes a suite of nine heteroleptic bis-cyclometalated iridium complexes, prepared by pairing the cyclometalating ligands piq and btp with five ancillary ligands. This work provides further insight into the influence of the ancillary ligand structure on the electrochemical and photophysical properties, highlighting the effects of replacing *N*-aryl substituents with alkyl groups, and of augmenting the steric profile of the ancillary ligand. Significantly, in a few of the compounds the modifications to the ancillary ligand lead to increases in k_r and/or decreases in k_{nr} relative to structurally related compounds, producing deep-red phosphors with photoluminescence quantum yields among the highest reported to date.

Results and Discussion

Synthesis of heteroleptic iridium complexes

The general synthetic procedure for the nine new complexes of type $Ir(C^N)_2(LX)$ (C^N = 1-phenylisoquinoline (piq) and 2-(2-pyridyl)benzothiophene (btp)) is described in Scheme 1. These two cyclometalating ligands are paired with five electron-rich ancillary ligands to prepare the new compounds described here, and Scheme 1 also summarizes three reference $Ir(piq)_2(L^X)$ compounds, **R1**–**R3**, which will be frequently referred to in this paper. In previous research we have extensively worked with *N*-phenyl-substituted β-diketiminate ($NacNac^{Me}$) and β-ketoiminate ($acNac^{Me}$) ancillary ligands.[17,42,44,45] To increase the steric profile we introduced methyl substituents at the *ortho* positions of the *N*-aryl groups in $(dmp)_2NacNac^{Me}$. Modifications to make the ancillary ligand more electron-rich include replacing backbone methyl groups with dimethylamino substituents ($NacNac^{NMe2}$), or replacing the *N*-phenyl substituent with a cyclohexyl ring in $(Cy)acNac^{Me}$. Similarly, we[42,43] and others[46–48] have used an amidinate

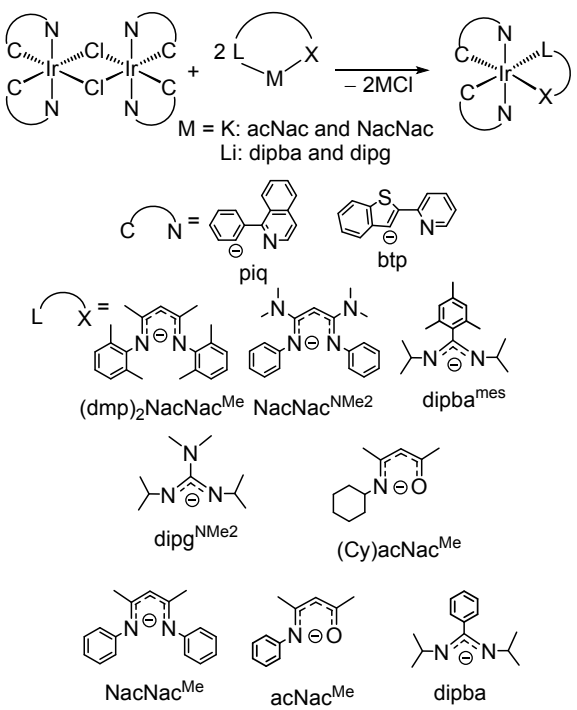

Compounds new to this work:
1a: C^N = piq, L^X = $(dmp)_2NacNac^{Me}$
1b: C^N = piq, L^X = $NacNac^{NMe2}$
1c: C^N = piq, L^X = $dipba^{mes}$
1d: C^N = piq, L^X = $dipg^{NMe2}$
1e: C^N = piq, L^X = $(Cy)acNac^{Me}$
2a: C^N = btp, L^X = $(dmp)_2NacNac^{Me}$
2b: C^N = btp, L^X = $NacNac^{NMe2}$
2c: C^N = btp, L^X = $dipba^{mes}$
2d: C^N = btp, L^X = $dipg^{NMe2}$
Reference compounds:
R1: C^N = piq, L^X = $NacNac^{Me}$
R2: C^N = piq, L^X = $acNac^{Me}$
R3: C^N = piq, L^X = dipba

Scheme 1. Synthesis of bis-cyclometalated iridium complexes.

ancillary ligand (dipba) in the design of bis-cyclometalated iridium complexes, and here we incorporate modifications to make the amidinate more sterically encumbered (dipba^{mes}), or make it more electron-rich by changing to a guanidinate (dipg^{NMe2}). The numbering scheme uses numerical designators for each C^N ligand (piq = **1**, and btp = **2**), with letters (**a**–**e**) denoting each L^X ligand. To prepare the complexes, the chloro-bridged dimers [Ir(C^N)$_2$(μ-Cl)]$_2$ were treated with (dmp)$_2$NacNac^{Me}K or NacNac^{NMe2}K at room temperature in THF to afford complexes **1a**–**b** and **2a**–**b** in moderate yields. A slightly different method was used to obtain complexes **1c**–**d** and **2c**–**d**, where the chloro-bridged dimers were treated with the in situ-generated lithium salt of dipba^{mes} and dipg^{NMe2} in tetrahydrofuran (THF) at 85 °C, whereas for **1e** the piq-ligated dimer was treated with (Cy)acNac^{Me}K in toluene at 130 °C. The identities of the complexes were verified by ^{1}H and ^{13}C{^{1}H} NMR, which also confirm the absence of any significant soluble impurities, except for small amounts of solvent in some cases. The NMR spectra evinced C_2 symmetry for all complexes except **1e**, where the asymmetric (Cy)acNac^{Me} ancillary ligand results in a C_1 point group, giving rise to distinct NMR resonances for each proton and carbon nucleus. The compounds are all chiral and are isolated as racemic mixtures, with NMR spectra showing the presence of a single product in each case, confirming the absence of any geometric isomers in the isolated products.

Structural characterization by X-ray crystallography

Complexes **1c**, **1d**, **2a**, **2b**, and **2d** were characterized by single crystal X-ray diffraction, with the structures depicted in Figures 1 and S1, and detailed crystallographic data reported in Tables S1–S2. Single crystals were grown via vapor diffusion of pentane into dichloromethane or tetrahydrofuran solution or by layering pentane onto a dichloromethane solution at room temperature inside the glovebox. The iridium atom is found to be at the center of a distorted octahedral geometry in all of the characterized structures, and we observe a trans disposition of the two nitrogen atoms of the cyclometalating ligands, as is typical for bis-cyclometalated iridium complexes.[7,17,42,43,49] Excepting NacNac^{NMe2} complex **2b**, where the NacNac core is "buckled" in a fashion analogous to other structurally

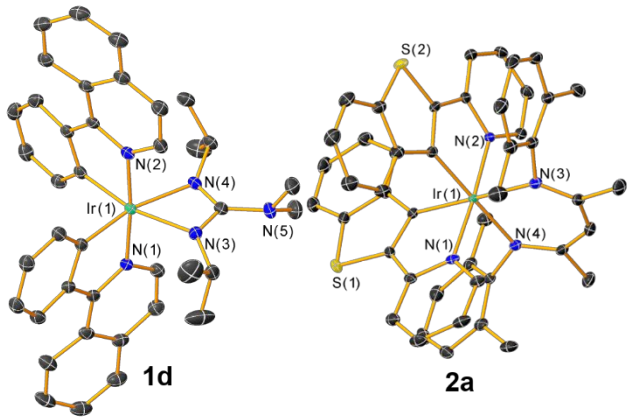

Figure 1. Molecular structures of complexes **1d** and **2a**, determined by single-crystal X-ray diffraction. Ellipsoids are depicted at 50% probability with hydrogen atoms and solvent molecules.

characterized NacNac^{NMe2} complexes from our group,[44,45] the ancillary ligand core and the chelated iridium atom are coplanar. The C–O, C–N, and C–C bond distances of the ancillary ligand chelate rings in all five characterized complexes are intermediate between typical single- and double-bond distances, suggesting a π-delocalized core. Unsurprisingly, the structure of the ancillary ligand determines the ancillary ligand N–C–N bite angle, which averages 60.49(10)° for complexes **1c**, **1d,** and **2d**, and is much larger in NacNac complexes **2b** (85.26(7)°) and **2a** (90.27(10)°).

The synthetic modifications we have made in this work, in an effort to make the ancillary ligands more sterically encumbered and/or more electron-rich, generally had only subtle effects on solid-state structural metrics. For example, (dmp)$_2$NacNac^{Me} complex **2a** shows a close approach of both N-aryl groups to a nearby Ir-aryl, in a nearly eclipsed orientation with apparent π–π stacking between the rings. This type of structural motif was also observed in several other iridium NacNac complexes previously described by our group, which lacked the *ortho*-methyl substituents.[17,50] In addition, comparison of previously reported Ir(btp)$_2$(dipba)[42] with complex **1c** shows that increased steric bulk on the amidinate's central aryl ring exerts only subtle influences on the structure. One small difference between these structures is an increase in the dihedral angle between the backbone aryl ring and the mean plane of the four-member chelate ring, which increases from 70.75° in the dipba complex to 81.58° in the mesityl-substituted complex **1c**. Similarly, the addition of electron-donating groups in dipg^{NMe2} complexes **1d** and **2d** does not demonstrably perturb the structures relative to the analogous amidinate complexes.

Electrochemical Properties

Figure 2 shows overlaid cyclic voltammograms of the complexes recorded in THF, with results summarized in Table 1. Figures S2 and S3 along with Table S3 collect the results of CV experiments conducted in MeCN. Redox potentials are reported relative to the ferrocenium/ferrocene (Fc^{+}/Fc) couple. All the complexes described in this work display a formally Ir^{IV}/Ir^{III} redox couple (E^{ox}), with potentials that are strongly dependent on the identity of the ancillary ligand. This couple is not completely reversible in some cases, with the return cathodic current notably less than the anodic current. If the CV is collected only in the positive direction, i.e. isolating the oxidation wave from the reduction(s), the reversibility is unaltered. The origin of this irreversibility is not entirely clear, though we have observed it in many other related compounds[42,43] and suspect it arises from decomposition of the ancillary ligand, since the HOMO in these compounds is majority ancillary ligand-centered.[42] Complexes supported by (dmp)$_2$NacNac^{Me}, **1a** and **2a**, have similar oxidation potentials (E^{ox} = −0.01 V and −0.02 V, respectively), close to the Fc^{+}/Fc couple. The electron-donating backbone dimethylamino groups in complexes **1b** and **2b** make the

molecules easier to oxidize, with potentials that are cathodically shifted by at least 160 mV. Addition of dimethylamino substituents in dipg^{NMe2} complexes **1d** and **2d**

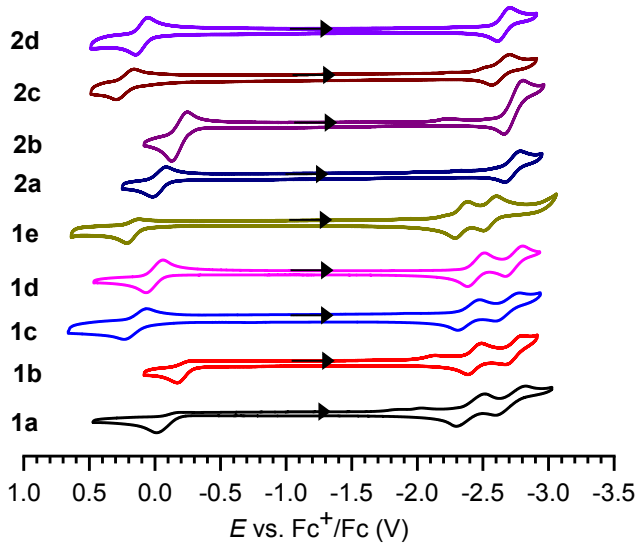

Figure 2. Overlaid cyclic voltammograms of complexes **1a**–**e** and **2a–d**. CVs were recorded in THF with 0.1 M NBu_4PF_6 supporting electrolyte, using a glassy carbon working electrode and a scan rate of 0.1 V/s. The arrows indicate the scan direction. Concentrations were not carefully controlled, and currents were normalized for better comparison.

resulted in a cathodic shift of 150 and 130 mV when compared to the amidinate complexes **1c** and **2c**, respectively.

Table 1. Summary of cyclic voltammetry data for all complexes

	(E vs. Fc$^+$/Fc) / V[a]	
C^N = piq (**1**)	E^{red}	E^{ox}
L^X = (dmp)$_2$NacNac^{Me} **(1a)**	−2.39, −2.70	−0.01[b]
L^X = NacNac^{Me2} **(1b)**	−2.43, −2.73	−0.17[b]
L^X = dipba^{mes} **(1c)**	−2.46, 2.61	+0.16
L^X = dipg^{NMe2} **(1d)**	−2.43, −2.73	+0.01
L^X = (Cy)acNac^{Me} **(1e)**	−2.32, 2.55	+0.22[b]
C^N = btp (**2**)		
L^X = (dmp)$_2$NacNac^{Me} **(2a)**	−2.72	−0.02
L^X = NacNac^{Me2} **(2b)**	−2.72	−0.19
L^X = dipba^{mes} **(2c)**	−2.63	0.23
L^X = dipg^{NMe2} **(2d)**	−2.66	0.10

[a] Experiments were performed in THF solvent with 0.1 M NBu_4PF_6 electrolyte with scan rate of 0.1 V/s using a glassy carbon working electrode and a silver wire pseudo-reference electrode. Potentials are referenced against the Fc$^+$/Fc redox couple. [b] Observed wave is irreversible, and the respective $E_{p,c}$ or $E_{p,a}$ peak potential is reported.

Another clear trend, which we have previously noted in other related complexes,[42,43] is that compounds with the smaller N–C–N bite angle, **1c/d** and **2c/d**, were more difficult to oxidize than the NacNac complexes. We believe this originates from the poorer overlap of ligand orbitals with the metal dπ orbitals in the small bite-angle analogues, resulting in less π donation into the d orbitals. Finally, complex **1e** (E^{ox} = +0.22 V) with a mixed *N,O* (Cy)acNac^{Me} chelate, was the most difficult to oxidize of the complexes in the piq series, and the reported potential is quite similar to the previously reported *N*-phenyl substituted complex Ir(piq)$_2$(acNac^{Me}) (**R2**),[42] suggesting that for the acNac ancillary ligand the basicity of the nitrogen donor is not particularly important for determining the HOMO energy and associated redox potential. To summarize, the trends in E^{ox} values indicate that the energy of the HOMO is strongly determined by the nature of the ancillary ligand, with associated redox potentials that span a wide range of >0.4 V.

The reduction potentials (E^{red}) of the new complexes described here depend only slightly on the identity of the L^X ligands. The two observed waves for the piq complexes are associated with sequential population of a π* orbital on each C^N ligand, with measured potentials beyond −2.0 V. We do note a minor "pre-feature" wave near –2.0 V in most complexes when the electrochemical studies were performed in acetonitrile (Figures S2 and S3), which arises irrespective of scan direction and we think can be attributed to the poor solubility in acetonitrile upon reduction, causing some deposition onto the electrode. As such the reported E^{red} values in Table S3 are for the one or two clearly-resolved waves that occur beyond this minor pre-feature. Consistent with this notion, this pre-feature wave was mostly absent when the CVs were recorded in THF. The first reduction potentials for all piq-ligated complexes were reversible, ranging from −2.32 V to −2.46 V in THF. Another subsequent reduction wave was observed for complexes **1a–e**, with potentials ranging between −2.55 (**1e**) and −2.73 (**1d**) V, reversible in most cases. All btp-ligated complexes display only one clearly-resolved reduction wave at a more negative potential than the piq series. In contrast to the HOMO energies, which are very dependent on the structure of the ancillary ligand, the observed reduction potentials of the new complexes indicate minimal perturbation of the C^N-centered LUMO energies across the series.

Photophysical Properties

The UV-vis absorption spectra and steady-state and time-resolved emission spectra of all the complexes were recorded in THF at room temperature. The UV-vis absorption spectra of complexes are depicted in Figures 3 and 4, along with the photoluminescence spectra discussed below. UV-vis absorption features and assignments are very similar to other bis-cyclometalated iridium complexes from our group with the same C^N ligands,[42,43] with intense absorption bands in the UV region assigned to spin-allowed ligand-centered π→π* transitions (^{1}LC) involving cyclometalating and ancillary ligands, and less intense, overlapping absorption bands tailing beyond 500 nm for btp (**2a–d**) and 600 nm for piq (**1a–e**) complexes assigned as both singlet and triplet metal-to-ligand charge transfer (^{1}MLCT/^{3}MLCT) transitions.

All of the complexes described here are luminescent at room temperature in deaerated THF solutions. Table 2 summarizes the steady-state and time-resolved emission data, and Figures 3 and 4 show overlaid room temperature emission spectra of **1** and **2** in THF along with emission spectra at 77 K in toluene. The excitation spectra of the new complexes were also collected and shown in Figures S4–S12, and in each case are superimposed with the absorption spectrum, indicating that luminescence arises solely from the iridium complex.

Our primary goal in this work is to produce complexes with improved deep-red photoluminescence attributes. The observed room-temperature emission for all of the complexes

Table 2. Summary of photoluminescence data for all complexes

	λ_{max} / nm[a] THF at 293 K	λ_{max} / nm[a] Toluene at 77 K	Φ_{PL}[b]	τ / μs[b]	k_r[c] × 10^{-5} / s^{-1} / k_{nr}[c] × 10^{-5} / s^{-1}
1a	660	642, 697	0.53	0.81	6.5/5.8
1b	707	666	0.071	0.25	2.8/37
1c	661	640, 699	0.58	0.74	7.8/5.6
1d	683	620, 678	0.37	0.53	6.8/11.8
1e	657	634, 687	0.49	0.78	6.2/6.6
2a	624	605, 664	0.27	4.0	0.68/1.8
2b	633	614, 668	0.18	2.8	0.63/2.9
2c	619, 668	609, 667	0.31	5.8	0.53/1.2
2d	626	611, 671	0.30	3.1	0.98/2.3

[a] λ_{ex} = 420 nm. [b] in THF at 293 K. [c] $k_r = \Phi/\tau$ and $k_{nr} = (1 - \Phi)/\tau$.

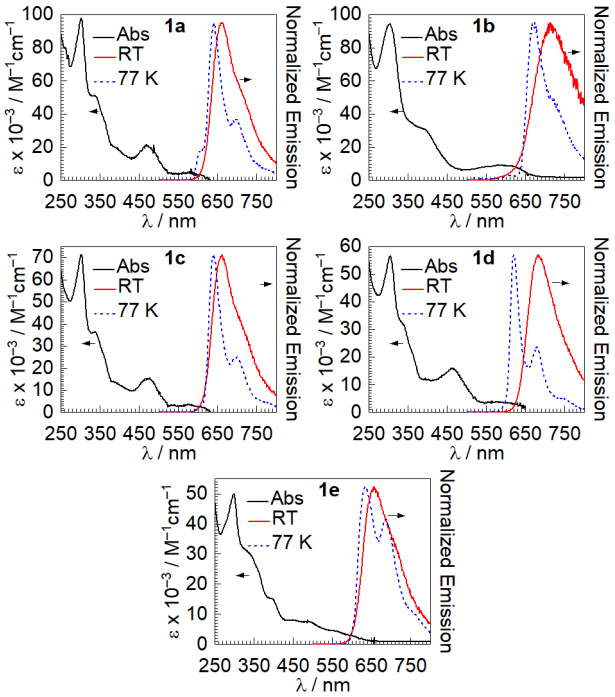

Figure 3. Overlaid UV-vis absorption (solid black line), room-temperature emission (red solid line), and 77-K emission (blue dashed line) spectra of complexes **1a–e**. UV-vis absorption and room-temperature emission were recorded in THF at room temperature, whereas the 77-K emission was recorded in frozen toluene glass. Samples were excited at λ_{ex} = 420 nm.

with C^N = piq occurs in the deep red portion of the spectrum, with maxima beyond 650 nm that are strongly dependent on the ancillary ligand. Two key observations are noted by examining the photoluminescence data of the piq series. First, we observe that making the ancillary ligand more electron-rich red-shifts the photoluminescence, offering a potential strategy for preparing near-infrared phosphors. In piq complexes there is substantial HOMO→LUMO character in the emissive T_1 state, and CV experiments (see above) show that the HOMO energies are significantly destabilized in the more electron-rich analogues. As a result, complexes with more electron-rich ancillary ligands have smaller HOMO–LUMO gaps and red-shifted photoluminescence. For example, the previously

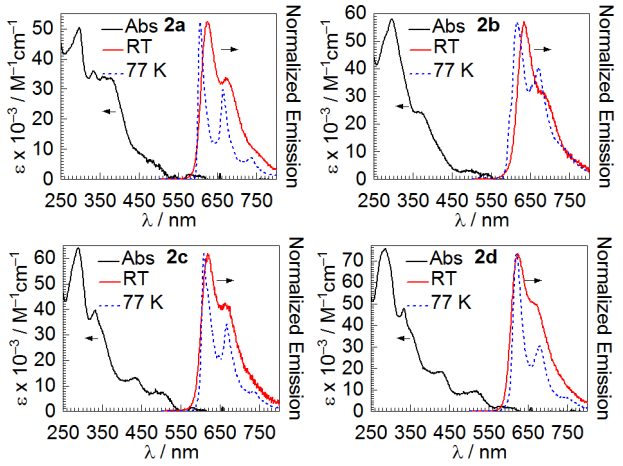

Figure 4. Overlaid UV-vis absorption (solid black line), room-temperature emission (red solid line), and 77-K emission (blue dashed line) spectra of complexes **2a–d**. UV-vis absorption and room-temperature emission were recorded in THF at room temperature, whereas the 77-K emission was recorded in frozen toluene glass. Samples were excited at λ_{ex} = 420 nm.

reported complex $Ir(piq)_2(NacNac^{Me})$ (**R1**)[42] has a photoluminescence λ_{max} of 678 nm, which shifts by 29 nm (605 cm^{-1}) to 707 nm, in dimethylamino-substituted **1b**. Complex **1b** is the only compound in the series that is truly in the NIR region (λ_{max} > 700 nm), but its modest photoluminescence quantum yield of 0.071 suggests that increasing the electron-richness of the ancillary ligand, while effective at producing NIR luminescence, may not be the best strategy for optimizing the quantum yield. Along the same lines, the complex $Ir(piq)_2(dipba^{mes})$ (**1c**) has a photoluminescence λ_{max} of 661 nm, which bathochromically shifts by 22 nm (487 cm^{-1}) in the more electron-rich $dipg^{NMe2}$ analogue **1d**.

The more significant outcome of this study is that certain structural modifications to the ancillary ligand can lead to larger Φ_{PL} values for the deep-red emitting $Ir(piq)_2(L^X)$ complexes, producing some of the most efficient deep-red phosphors ever

reported. In studying the deep-red phosphorescent compounds **R1** and **R3**, we noted modest photoluminescence quantum efficiencies on account of rather large k_{nr} values, as predicted by the energy-gap law. Our hypothesis leading into this work was that rigidifying the ancillary ligand, by adding sterically encumbering substituents, could lead to a suppression of k_{nr} and an increase in Φ_{PL}. This hypothesis was examined by preparing compounds **1a** and **1c**, more sterically crowded analogues of **R1** and **R3**. NacNac^{Me} compound **R1** has a photoluminescence λ_{max} of 678 nm and a Φ_{PL} of 0.17, and in **1a** we observe a blue-shift to 660 nm, but a significant increase in quantum yield to 0.53. Similarly, dipba compound **R3** emits at 671 nm with a quantum yield of 0.34, and in **1c** the photoluminescence is mildly blue-shifted to 661 nm but the quantum yield is much higher at 0.58. The increases in quantum yield are to some extent a result of a decrease in k_{nr}, with a ca. 40% reduction in each case, but unexpectedly the more structurally rigid analogues **1a** and **1c** also exhibited larger radiative rate constants (k_r), which increased by a factor of 3.1 (**R1** to **1a**) and 1.7 (**R3** to **1c**). Thus, both an increase in k_r and a decrease in k_{nr} led to the higher quantum yields observed in sterically encumbered complexes **1a** and **1c**. We hypothesize that the slight blue-shift in complexes **1a** and **1c**, relative to **R1** and **R3**, is a result of the more sterically crowded ancillary ligand leading to a less distorted T_1 state, reducing the singlet-triplet gap. We also discovered, by preparing (Cy)acNac^{Me} complex **1e**, that incorporation of *N*-alkyl substituents onto a β-ketoiminate can also be an effective strategy for deep-red luminescence, with complex **1e** exhibiting a λ_{max} of 657 nm and a quantum yield of 0.49.

Taken together, these results not only unveiled several structure-property relationships, but also led to the discovery of a few top-performing deep-red phosphors that are significantly more efficient than previous analogues prepared by our group. We have three new compounds, **1a**, **1c**, and **1e** where the photoluminescence maximum is beyond 650 nm and the quantum yield is 0.49 or greater, and a fourth compound, **1d**, where the luminescence is very deep in the red (λ_{max} = 683 nm) and the quantum yield is still a respectable value, 0.37. There are some platinum complexes in the literature with quantum yields that rival or surpass the compounds introduced here, including some tetradentate cyclometalated platinum complexes with deep-red to NIR excimer emission with Φ_{PL} as high as 0.74 in neat films,[38] and a diplatinum complex with phosphorescence in the red region (λ_{max} = 607 nm) and a quantum yield of 0.75.[37] That said, the new compounds in this work all have higher quantum yields than some of the best-known deep-red phosphorescent iridium compounds in the literature. For example, Ir(C^N)$_2$(acac) (acac = acetylacetonate) compounds where C^N is an 8-phenylquinoline derivative, an isomer of piq, luminesce in the deep red (λ_{max} = 650–680 nm) but with a maximum Φ_{PL} of 0.11.[51] In addition, a picolinate supported bis-cyclometalated iridium complex with C^N = 6-phenylphenanthridine, a π-extended analogue of piq, luminesces with λ_{max} = 648 nm and Φ_{PL} = 0.27.[52] Some recent improvements have been made by introducing new C^N ligands, sticking exclusively with acac or picolinate-supported bis-cyclometalated iridium structures. These include an Ir(C^N)$_2$(acac) complex with phenazine-derived C^N ligands (λ_{max} = 684 nm and Φ_{PL} = 0.27),[53] an Ir(C^N)$_2$(acac) compound with spirofluorene-dibenzosuberene[d]quinoxaline C^N ligands (λ_{max} = 686 nm and Φ_{PL} = 0.51), and finally two picolinate-supported complexes with benzo[b]thiophen-2-yl)quinoline C^N ligands, π-extended versions of btp (λ_{max} = 651 and 661 nm, and Φ_{PL} = 0.48 and 0.37, respectively).[54] Clearly, there has been a surge of interest in preparing efficient deep-red iridium phosphors and applying them in optoelectronic devices, and the compounds described here offer a complementary approach to accessing deep-red emitters and have photoluminescence attributes that rival or exceed these recent breakthrough examples.

As part of this study we prepared four compounds with C^N = btp, another cyclometalating ligand known to engender red phosphorescence. In most cases, our previous work with Ir(btp)$_2$(L^X) compounds showed that in these compounds the photoluminescence wavelength and excited-state dynamics were not responsive to the structure of the ancillary ligand.[42,43] A notable exception is the compound Ir(btp)$_2$(dipba), which has a slightly redder photoluminescence (λ_{max} = 622 nm) and much higher quantum yield (0.79) than most other Ir(btp)$_2$(L^X) compounds, but in almost every other case the emission wavelength was ~610 nm and the quantum yield in the narrow range of 0.2–0.3. We prepared compounds **2a**–**2d** to examine whether ancillary ligands which are even more sterically encumbered or even more electron rich could influence the photoluminescence in a meaningful way. But as the data in Figure 4 and Table 2 show, the photoluminescence attributes of complexes **2a**–**2d** are all quite similar. We do see a modest red-shift of the photoluminescence in these compounds, by 7–21 nm (185–542 cm^{-1}) relative to Ir(btp)$_2$(acac),[7] but in no case is there an increase in quantum yield. We believe this difference in behavior between piq and btp complexes arises from the larger singlet-triplet gap in the latter's C^N ligand-centered state, leading to less excited-state MLCT character and thus less influence of the electron-rich ancillary ligand. Acknowledging that the excited-state dynamics of compounds with C^N = btp are more difficult to influence, we believe going forward that a better strategy for continued development of deep-red and NIR emitters will be to use C^N ligands akin to piq, where the cyclometalated aryl ring is a phenyl group and the ancillary ligand is expected to have a much more profound influence on the spectral profile and photoluminescence kinetics.

Further insight into the photoluminescence comes from low-temperature (77 K) emission spectra of the complexes, which are also shown in Figures 3 and 4. These low-temperature spectra are reproduced in Figures S13–S21, overlaid with the room-temperature spectrum. Complexes with C^N = piq, **1a**–**e**, have poorly resolved vibronic structure at room temperature, but in most cases, excepting the electron-rich NacNac complex **1b**, two distinct vibronic maxima can be resolved at 77 K in toluene glass (Figure 3). The vibronic spacing for this series of compounds falls in the range of ca. 1216–1379 cm^{-1}. Also evident in the piq series is a large rigidochromic blue-shift (Figures S13–S17), which we[17,42,43] and many others[55] have

previously noted is evidence for significant charge-transfer character in the emissive T_1 state. Better-resolved emission spectra were observed for btp complexes at 77 K, with smaller rigidochromic shifts averaging 15 nm (ca. 400 cm^{-1}) (Table 2 and Figures S18–S21). The vibronic spacing in the btp complexes is larger in most cases, at parity of ancillary ligand, and falls in the range of ca. 1316–1468 cm^{-1}.

Conclusions

We have presented here a thorough study of the effect of ancillary ligand modification on the electrochemical and optical properties of bis-cyclometalated iridium complexes, focusing in particular on the effects of electron-donating and sterically encumbering substituents. Our primary goal in this work was to improve the quantum yields of deep-red emitting complexes. Appropriate electronic tuning of the ancillary ligand in $Ir(piq)_2(L\text{^}X)$ complexes begets luminesce in the deep-red region (λ_{max} > 650 nm), and increasing the steric profile of the ancillary ligand can produce photoluminescence quantum yields >0.5, among the highest for deep-red phosphorescence. With the most extremely electron-rich ancillary ligand $NacNac^{NMe2}$ the photoluminescence is perturbed all the way to NIR region (λ_{max} > 700 nm), although the quantum yield is modest. A smaller series of compounds with C^N = btp were also prepared, but in these cases the photoluminescence wavelength and the excited-state dynamics are minimally sensitive to the structure of the ancillary ligand, and only red-emitting compounds with modest quantum yields (~0.2–0.3) were produced. Taken together, these results show that our strategy of using electron-rich ancillary ligands is successful at producing some of the best-performing deep-red emitters available. Our future goals are to apply the strategy described here to significantly improve quantum yields for NIR phosphors, in particular in compounds with phenyl-bound C^N ligands where the excited-state dynamics are expected to be particularly sensitive to the ancillary ligand structure.

Experimental Section

Materials: Starting materials and reagents were of commercial origin and used without further purification. All reactions were executed in a nitrogen-filled glovebox operating at <1 ppm of O_2 and H_2O. Anhydrous solvents for reactions and optical measurements were dried by the method of Grubbs,[56] passing through dual alumina columns on a commercial solvent purification system (SPS), and stored over 3 Å molecular sieves. All NMR solvents were dried and stored over 3 Å molecular sieves in the glovebox; $CDCl_3$ was also stored over potassium carbonate in addition to sieves. Cyclometalated iridium dimers $[Ir(C\text{^}N)_2(\mu\text{-}Cl)]_2$ (C^N = 1-phenylisoquinoline (piq) and 2-(2-pyridyl)benzothiophene (btp)) were prepared by the method of Nonoyama,[57] refluxing $IrCl_3{\cdot}nH_2O$ with 2–2.3 equiv of the cyclometalating ligand in a 3:1 mixture of 2-ethoxyethanol and water. Potassium or lithium salts of the acNac and NacNac ligands were prepared by the general procedure as described previously by our lab.[17] Tetrabutylammonium hexafluorophosphate ($TBAPF_6$) was recrystallized from hot ethanol and ferrocene was sublimed before use in electrochemical experiments.

Physical Methods: ^1H and $^{13}C\{^1H\}$ NMR spectra were recorded at room temperature using a JEOL ECA-400, ECA-500, or ECA-600 NMR spectrometer. UV–vis absorption spectra were recorded in THF solution in screw-capped quartz cuvettes using an Agilent Carey 8454 UV–vis spectrophotometer. Luminescence lifetimes were measured with a Horiba DeltaFlex Lifetime System, using 390 nm pulsed diode excitation. Steady-state emission spectra were recorded using a Horiba FluoroMax-4 spectrofluorometer with appropriate long-pass filters to exclude stray excitation light from detection. In order to exclude air, samples for emission spectra were prepared in a nitrogen-filled glovebox using anhydrous solvents. Samples for room-temperature emission were housed in 1 cm quartz cuvettes with septum-sealed screw caps, and samples for low-temperature emission were contained in a custom quartz EPR tube with high-vacuum valve and immersed in liquid nitrogen using a finger dewar. Solution quantum yields were determined relative to a standard of tetraphenylporphyrin in toluene, which has a reported fluorescence quantum yield (Φ_{PL}) of 0.11.[58] Cyclic voltammetry (CV) measurements were performed with a CH Instruments 602E potentiostat interfaced with a nitrogen glovebox via wire feedthroughs. Samples were dissolved in acetonitrile or THF with 0.1 M $TBAPF_6$ as a supporting electrolyte. A 3 mm diameter glassy-carbon working electrode, a platinum wire counter electrode, and a silver wire pseudo-reference electrode were used. Potentials were referenced to an internal standard of ferrocene.

Preparation of (Cy)acNac^{Me}H. Acetylacetone (5.00 g, 50 mmol, 1.0 equiv) and cyclohexylamine (4.46 g, 45 mmol, 0.9 equiv) were dissolved into 20 mL of DCM and the solution was stirred at room-temperature for two days. To the opaque, yellow mixture 20 mL of water were added and the organic layer was separated and dried over Na_2SO_4. The solvent was removed under reduced pressure and gave a yellow liquid. Analysis by ^1H NMR spectroscopy (Figure S31) indicated sufficient purity for further use. Yield 5.59 g (69%). ^1H-NMR (400 MHz, $CDCl_3$) δ: 10.97 (bs, 1H, N*H*), 4.89 (s, 1H, (C=O)C*H*(C=N)), 3.32-3.37 (m, 1H, Cy*H*), 1.97 (s, 3H, CH_3), 1.92 (s, 3H, CH_3), 1.75-1.87 (m, 4H, Cy*H*), 1.50-1.58 (m, 1H, Cy*H*), 1.23-1.37 (m, 5H, Cy*H*).

Preparation of Ir(piq)$_2$[(dmp)$_2$NacNac^{Me}] (1a). In the glovebox, $[Ir(piq)_2(\mu\text{-}Cl)]_2$ (50 mg, 0.039 mmol) was suspended in 3 mL THF, and a solution of $(dmp)_2NacNac^{Me}K$ (29 mg, 0.089 mmol, 2.3 equiv) in 5 mL THF was added to the dimer suspension slowly by pipet. The resulting reddish-brown mixture was stirred overnight at room temperature, during which time the color of the solution changed to dark red. The solvent was removed under reduced pressure, and the resulting residue was extracted with 5 mL of toluene and filtered through Celite to remove KCl and other insoluble impurities. The toluene was removed in vacuo, and the residue was washed with 2 × 3 mL of room-temperature Et_2O. The final product was obtained by adding pentane to a concentrated DCM solution which was dried under vacuum. Yield: 37 mg (53%). ^1H NMR (600 MHz,

$CDCl_3$) δ: 9.23 (d, *J* = 6.2 Hz, 2H, Ar*H*), 8.57 (d, *J* = 8.9 Hz, 2H, Ar*H*), 7.89 (d, *J* = 8.2 Hz, 2H, Ar*H*), 7.64–7.72 (m, 4H, Ar*H*), 7.60 (t, *J* = 7.6 Hz, 2H, Ar*H*), 7.42 (d, *J* = 6.2 Hz, 2H, Ar*H*), 6.56–6.67 (m, 6H, Ar*H*), 6.17–6.29 (m, 4H, Ar*H*), 5.99 (d, *J* = 7.6 Hz, 2H, Ar*H*), 4.79 (s, 1H, $(Me)_2$PhNC(Me)C*H*C(Me)NPh$(Me)_2$), 2.04 (s, 6H, CH_3), 1.51 (s, 6H, CH_3), 0.875 (s, 6H, CH_3). $^{13}C\{^1H\}$ NMR (151 MHz, $CDCl_3$) δ: 171.3, 159.8, 155.2, 149.7, 146.5, 146.3, 136.8, 133.0, 132.7, 131.7, 130.5, 129.2, 128.1, 127.8, 127.5, 127.4, 127.3, 126.5, 126.4, 125.7, 122.7, 119.6, 117.5, 96.74, 25.26, 21.53, 17.02. UV-vis (THF): λ/nm (ε/M^{-1} cm^{-1}) 302(98000), 343(sh)(50000), 390(sh)(20000), 468(21000).

Preparation of Ir(piq)$_2$(NacNac^{NMe2}) (1b). In the glovebox, $[Ir(piq)_2(\mu\text{-}Cl)]_2$ (60 mg, 0.047 mmol) was suspended in 3 mL of THF, and a solution of NacNac^{NMe2}K (35 mg, 0.010 mmol, 2.2 equiv) in 5 mL of THF was added to the dimer suspension slowly by pipet. The resulting reddish orange mixture was stirred overnight at room temperature, during which time the color of the solution changed to dark green. The solvent was removed under reduced pressure, and the resulting residue was extracted with 5 mL of toluene and filtered through Celite to remove KCl and other insoluble impurities. The toluene was removed in vacuo, and the residue was washed with 2 × 3 mL of room-temperature Et_2O. Final product was obtained by adding pentane to a concentrated DCM solution which was dried under vacuum. Yield: 62 mg (73%). ^1H NMR (400 MHz, $CDCl_3$) δ: 8.73 (d, *J* = 8.9 Hz, 2H, Ar*H*), 8.51 (d, *J* = 6.9 Hz, 2H, Ar*H*), 8.03 (d, *J* = 8.2 Hz, 2H, Ar*H*), 7.71 (d, *J* = 8.2 Hz, 2H, Ar*H*), 7.47–7.58 (m, 4H, Ar*H*), 6.96 (d, *J* = 6.2 Hz, 2H, Ar*H*), 6.85 (t, *J* = 7.6 Hz, 2H, Ar*H*), 6.47–6.65 (m, 8H, Ar*H*), 6.32 (t, *J* = 7.6 Hz, 2H, Ar*H*), 6.04 (d, *J* = 8.2 Hz, 4H, Ar*H*), 3.83 (s, 1H, PhNC(NMe_2)C*H*C(NMe_2)NPh), 2.29 (s, 12H, CH_3). $^{13}C\{^1H\}$ NMR (151 MHz, $CDCl_3$) δ: 170.1, 167.8, 162.3, 153.8, 146.2, 144.6, 136.5, 133.2, 130.2, 129.9, 128.2, 127.1, 127.0, 126.5, 126.2, 125.7, 125.6, 119.4, 119.3, 117.0, 86.17, 40.99. UV-vis (THF): λ/nm (ε/M^{-1} cm^{-1}) 302(94000), 370(sh)(24000), 579(9300).

Preparation of Ir(piq)$_2$(dipba^{mes}) (1c). In the glovebox, 2-bromomesitylene (36 mg, 0.18 mmol) was dissolved in 5 mL THF and the solution was kept at −35° C for 1 h. After that a hexane solution of *n*-BuLi (~0.11 mL, 1.6 M) was added, and the reaction mixture was stirred at −35 °C for 10 min. Then *N,N*′-diisopropylcarbodiimide (23 mg, 0.18 mmol) was added to the solution and the reaction mixture was stirred at room temperature for another 10 min. The colorless solution was then added dropwise to a Teflon-capped glass tube containing $[Ir(piq)_2(\mu\text{-}Cl)]_2$ (100 mg, 0.0786 mmol) in 5 mL THF. The resulting reddish orange mixture was stirred overnight outside of glovebox at 80–85 °C, during which time the color of the solution changed to dark brown. The mixture was cooled to room temperature and the sealed tube was taken inside the glovebox for further workup procedure. The solvent was removed under reduced pressure and the residue was extracted in 2 mL toluene and evaporated under reduced pressure to remove THF completely. The product was redissolved in 10mL toluene and filtered through Celite to remove LiCl and other insoluble impurities. The crude product was washed with 3 × 3 mL of Et_2O and 2 × 3 of mL hexane. The solid was redissolved in minimum amount of DCM and pentane was added to slowly induce precipitation and the resulted reddish-brown solid was concentrated to dryness. Yield: 55 mg (48%). ^1H NMR (600 MHz, $CDCl_3$) δ: 9.55 (d, *J* = 6.4 Hz, 2H, Ar*H*), 8.96 (d, *J* = 8.2 Hz, 2H, Ar*H*), 8.17 (d, *J* = 7.8 Hz, 2H, Ar*H*), 7.96 (d, *J* = 7.3 Hz, 2H, Ar*H*), 7.63–7.75 (m, 4H, Ar*H*), 7.53 (d, *J* = 6.4 Hz, 2H, Ar*H*), 6.77–6.93 (m, 4H, Ar*H*), 6.61–6.67 (m, 2H, Ar*H*), 6.36 (d, *J* = 7.8 Hz, 2H, Ar*H*), 3.04 (sept, *J* = 6.2 Hz, 2H, $(CH_3)_2$C*H*N), 2.43 (s, 6H, CH_3), 2.25 (s, 3H, CH_3), 0.72 (d, *J* = 5.6 Hz, 6H, CH_3), −0.06 (d, *J* = 6.4 Hz, 6H, CH_3). $^{13}C\{^1H\}$ NMR (151 MHz, $CDCl_3$) δ: 173.0, 170.1, 159.5, 146.3, 145.8, 137.2, 136.5, 136.2, 133.7, 132.6, 130.2, 129.7, 128.8, 128.3, 127.3, 127.2, 127.1, 126.2, 119.2, 119.0, 48.73, 25.17, 24.88, 21.33, 21.14. UV-vis (THF): λ/nm (ε/M^{-1} cm^{-1}) 302(87000), 337(44000), 393(sh)(16000), 476(19000), 582(sh)(4000).

Preparation of Ir(piq)$_2$(dipg^{NMe2}) (1d). In the glovebox, lithium dimethylamide (~4 mg, 0.08 mmol) was dissolved in 5 mL THF and the solution was kept at −35 °C for 1 h. After that *N,N*′-diisopropylcarbodiimide (11 mg, 0.083 mmol) was added to the solution and the mixture was stirred at room temp for 30 min. The colorless guanidinate solution was then added dropwise to the Teflon-capped glass tube containing $[Ir(piq)_2(\mu\text{-}Cl)]_2$ (50 mg, 0.039 mmol) in 5 mL THF. The resulting red mixture was stirred overnight outside of the glovebox at 80–85 °C, during which time the color of the solution changed to light brown. The mixture was cooled to room temperature and the sealed tube was taken inside the glovebox for further workup procedure. The solvent was removed under reduced pressure and the residue was extracted in 3 mL of toluene and evaporated under reduced pressure to remove THF completely. The product was redissolved in 5 mL of toluene and filtered through Celite to remove LiCl and other insoluble impurities. The crude product was washed with 3 × 3 mL of Et_2O and 2 × 3 mL of pentane. The crude product was redissolved in minimum amount of THF and pentane was added to the solution to slowly induced precipitation. The light brown solid was washed again with 2 × 2 mL of Et_2O and the resulting solution was concentrated to dryness. Yield: 33 mg (54%). ^1H NMR (600 MHz, $CDCl_3$) δ: 9.32 (d, *J* = 6.3 Hz, 2H, Ar*H*), 8.92 (d, *J* = 8.0 Hz, 2H, Ar*H*), 8.13 (d, *J* = 8.0 Hz, 2H, Ar*H*), 7.93 (d, *J* = 7.4 Hz, 2H, Ar*H*), 7.59–7.76 (m, 4H, Ar*H*), 7.48 (d, *J* = 6.3 Hz, 2H, Ar*H*), 6.80 (t, *J* = 7.4 Hz, 2H, Ar*H*), 6.56 (d, *J* = 6.9 Hz, 2H, Ar*H*), 6.22 (d, *J* = 7.4 Hz, 2H, Ar*H*), 3.71 (sept, *J*= 6.3 Hz, 2H, $(CH_3)_2$C*H*N), 2.86 (s, 6H, CH_3), 0.57 (d, *J* = 6.3 Hz, 6H, CH_3), −0.05 (d, *J* = 6.3 Hz, 6H, CH_3). $^{13}C\{^1H\}$ NMR (151 MHz, $CDCl_3$) δ: 170.2, 169.9, 161.2, 146.2, 143.3, 136.2, 132.6, 130.0, 129.8, 128.7, 127.2, 127.1, 126.4, 119.1, 118.9, 47.66, 40.77, 24.79, 24.33. UV-vis (THF): λ/nm (ε/M^{-1} cm^{-1}) 305(57000), 341(sh)(31000), 464(16000), 583(sh)(4000).

Preparation of Ir(piq)$_2$[(Cy)acNac^{Me}] (1e). In the glovebox, $[Ir(piq)_2(\mu\text{-}Cl)]_2$ (100 mg, 0.079 mmol) was suspended in 5 mL of toluene in a Teflon-capped glass tube. A suspension of (Cy)acNac^{Me}K (33 mg, 0.15 mmol) in 5 mL of toluene was added into the tube slowly via pipette. The reaction mixture was heated outside of glovebox at 130 °C for five days. The mixture was cooled to room temperature and the sealed tube was taken inside the glovebox for further workup procedure. The resulting dark red mixture was filtered through Celite and concentrated in vacuo. The residue was crystallized using 2 mL of Et_2O at

−35 °C. The supernatant liquid was removed via pipette and the solid residue was washed again with 2 × 3 mL of cold Et_2O and 3 × 3 mL of pentane. The resulting solid was dried in vacuo and obtained as dark red solid. Yield: 41 mg (35%). ^{1}H-NMR (400 MHz, CD_2Cl_2) *δ*: 8.98–9.04 (m, 1H, Ar*H*), 8.92 (d, *J* = 7.8 Hz, 1H, Ar*H*), 8.75 (q, *J* = 6.6 Hz, 2H, Ar*H*), 8.30 (d, *J* = 8.2 Hz, 1H, Ar*H*), 8.15 (d, *J* = 7.8 Hz, 1H, Ar*H*), 7.92–7.99 (m, 2H, Ar*H*), 7.66–7.75 (m, 4H, Ar*H*), 7.48 (dd, *J* = 6.4, 29 Hz, 2H, Ar*H*), 6.91 (q, *J* = 7.2 Hz, 2H, Ar*H*), 6.58–6.70 (m, 2H, Ar*H*), 6.45 (d, *J* = 7.8 Hz, 1H, Ar*H*), 6.19 (d, *J* = 6.9 Hz, 1H, Ar*H*), 4.56 (s, 1H, CyNC(Me)C*H*C(O)Me), 3.06 (s, 1H, Cy*H*), 1.99 (s, 3H, CH_3), 1.65 (br s, 1H, Cy*H*) 1.59 (s, 3H, CH_3), 0.96–1.43 (m, 5H, Cy*H*), 0.60–0.92 (m, 1H, Cy*H*), 0.01–0.48 (m, 3H, Cy*H*). ^{13}C{^{1}H} NMR (126 MHz, CD_2Cl_2) *δ*: 173.73, 169.38, 168.70, 163.12, 158.47, 157.57, 147.01, 146.22, 142.97, 141.42, 137.03, 136.89, 133.16, 132.33, 130.59, 130.56, 130.34, 129.63, 129.07, 128.30, 127.75, 127.52, 127.04, 126.94, 126.46, 126.41, 126.32, 120.55, 119.83, 119.37, 99.77, 66.07, 32.40, 31.97, 26.51, 26.21, 25.73. UV-vis (THF): λ/nm (ε/M^{-1} cm^{-1}) 298(50000), 322(sh)(32000), 384(sh)(16000), 486(7100).

Preparation of Ir(btp)$_2$[(dmp)$_2$NacNac^{Me}] (2a). Prepared by the method described above for complex **1a**, using [Ir(btp)$_2$(μ-Cl)$_2$] (50 mg, 0.038 mmol) and (dmp)$_2$NacNac^{Me}K (30 mg, 0.089 mmol). The purified product was a dark orange colored solid. Yield: 43 mg (63%). ^{1}H NMR (600 MHz, $CDCl_3$) δ: 9.24 (d, *J* = 6.2 Hz, 2H, Ar*H*), 7.70 (t, *J* = 7.6 Hz, 2H, Ar*H*), 7.33 (d, *J* = 7.6 Hz, 2H, Ar*H*), 7.27 (d, *J* = 7.6 Hz, 2H, Ar*H*), 7.03 (t, *J* = 6.2 Hz, 2H, Ar*H*), 6.86 (t, *J* = 6.9 Hz, 2H, Ar*H*), 6.57 (t, *J* = 7.6 Hz, 2H, Ar*H*), 6.38–6.47 (m, 4H, Ar*H*), 5.95 (d, *J* = 6.9 Hz, 2H, Ar*H*), 5.90 (d, *J* = 8.3 Hz, 2H, Ar*H*), 4.79 (s, 1H, (Me)$_2$PhNC(Me)C*H*C(Me)NPh(Me)$_2$), 1.82 (s, 6H, CH_3), 1.68 (s, 6H, CH_3), 1.32 (s, 6H, CH_3). ^{13}C{^{1}H} NMR (151 MHz, $CDCl_3$): 167.5, 159.2, 155.0, 152.5, 148.5, 146.1, 142.4, 137.6, 136.0, 133.0, 132.6, 127.4, 126.9, 126.0, 124.0, 123.4, 122.2, 122.0, 117.5, 117.4, 98.08, 25.61, 23.88, 17.53. UV-vis (THF): λ/nm (ε/M^{-1} cm^{-1}) 297(51000), 332(36000), 359(33000), 383(sh)(32000), 498(sh)(5000).

Preparation of Ir(btp)$_2$(NacNac^{NMe2}) (2b). Prepared by the method described above for complex **1b**, using [Ir(btp)$_2$(μ-Cl)$_2$] (50 mg, 0.038 mmol) and (dmp)$_2$NacNac^{Me}K (27 mg, 0.078 mmol, 2.1 equiv). The purified product was a light orange colored solid. Yield: 35 mg (50%). ^{1}H NMR (400 MHz, $CDCl_3$) δ: 8.75 (d, *J* = 5.5 Hz, 2H, Ar*H*), 7.60 (d, *J* = 8.2 Hz, 2H, Ar*H*), 7.43 (t, *J* = 6.9 Hz, 2H, Ar*H*), 7.13–7.17 (m, 2H, Ar*H*), 6.99 (t, *J* = 8.2 Hz, 2H, Ar*H*), 6.66–6.76 (m, 4H, Ar*H*), 6.44–6.58 (m, 6H, Ar*H*), 6.09 (d, *J* = 8.2 Hz, 2H, Ar*H*), 5.96 (d, *J* = 7.6 Hz, 4H, Ar*H*), 4.06 (s, 1H, PhNC(NMe$_2$)C*H*C(NMe$_2$)NPh), 2.38 (s, 12H, CH_3). ^{13}C{^{1}H} NMR (151 MHz, $CDCl_3$) δ: 167.1, 166.7, 155.4, 152.4, 151.1, 147.4, 142.5, 136.7, 135.0, 129.1, 128.3, 127.1, 126.3, 126.1, 124.4, 123.2, 122.5, 119.6, 117.2, 116.9, 84.61, 41.21. UV-vis (THF): λ/nm (ε/M^{-1} cm^{-1}) 296(58000), 370(sh)(24000), 500(4000).

Preparation of Ir(btp)$_2$(dipba^{mes}) (2c). In the glovebox, 2-bromomesitylene (~33 mg, 0.17 mmol) was dissolved in 5 mL THF and the solution was kept at −35° C for 1 h. After that a hexane solution of *n*-BuLi (~0.11 mL, 1.6 M) was added, and the reaction mixture was stirred at −35° C for 10 min. Then *N,N*′-diisopropylcarbodiimide (~21 mg, 0.17 mmol) was added to the solution and the reaction mixture was stirred at room temp for 10 min. The colorless solution was then added dropwise to the Teflon-capped glass tube containing [Ir(btp)$_2$(μ-Cl)]$_2$ (100 mg, 0.0769 mmol) in 5 mL of THF. The resulting yellow mixture was stirred overnight outside of glovebox at 80–85 °C, during which time the color of the solution changed to light orange. The mixture was cooled to room temperature and the sealed tube was taken inside the glovebox for further workup procedure. The solvent was removed under reduced pressure and the residue was extracted into 3 mL of toluene and evaporated under reduced pressure to remove THF completely. The product was redissolved in 15 mL of toluene and filtered through Celite to remove LiCl and other insoluble impurities. The crude product was washed with 3 × 3 mL of Et_2O and 2 × 3 of mL hexane. The solid was redissolved in minimum amount of DCM and pentane was added to slowly induce precipitation and the resulted orange solid was concentrated to dryness. Yield: 42 mg (32%). ^{1}H NMR (600 MHz, $CDCl_3$) δ: 9.52 (d, *J* = 5.5 Hz, 2H, Ar*H*), 7.77 (t, *J* = 7.9 Hz, 2H, Ar*H*), 7.63 (dd, *J* = 7.6, 35 Hz, 4H, Ar*H*), 7.01–7.11 (m, 4H, Ar*H*), 6.76–6.88 (m, 4H, Ar*H*), 6.21 (d, *J* = 8.2 Hz, 2H, Ar*H*), 2.96 (sept, *J* = 6.2 Hz, 2H, (CH$_3$)$_2$C*H*N), 2.37 (s, 6H, CH_3), 2.25 (s, 3H, CH$_3$), 0.59 (d, *J* = 6.2 Hz, 6H, CH_3), 0.07 (d, *J* = 6.2 Hz, 6H, CH_3). ^{13}C{^{1}H} NMR (151 MHz, $CDCl_3$) δ: 174.3, 167.1, 154.4, 153.5, 147.6, 142.7, 137.7, 136.9, 136.0, 134.5, 132.7, 128.6, 126.0, 124.7, 123.4, 122.7, 117.4, 117.6, 48.08, 24.75, 24.55, 21.54, 21.15. UV-vis (THF): λ/nm (ε/M^{-1} cm^{-1}) 288(64000), 331(40000), 432(13000), 486(sh)(8000), 583(sh)(1000).

Preparation of Ir(btp)$_2$(dipg^{NMe2}) (2d). Prepared by the method described above for complex **1d**, using [Ir(btp)$_2$(μ-Cl)$_2$] (100 mg, 0.0768 mmol), lithium dimethylamide (~8 mg, 0.16 mmol, 2.1 equiv), and *N,N*′-diisopropylcarbodiimide (~20 mg, 0.16 mmol). The purified product was a light orange colored solid. Yield: 61 mg (51%). ^{1}H NMR (600 MHz, $CDCl_3$) δ: 9.26 (d, *J* = 5.5 Hz, 2H, Ar*H*), 7.69 (t, *J* = 7.5 Hz, 2H, Ar*H*), 7.61 (d, *J* = 8.4 Hz, 2H, Ar*H*), 7.55 (d, *J* = 7.8 Hz, 2H, Ar*H*), 6.97–7.07 (m, 4H, Ar*H*), 6.76 (t, *J* = 7.6 Hz, 2H, Ar*H*), 6.16 (d, *J* = 7.6 Hz, 2H, Ar*H*), 3.60 (sept, *J* = 6.2 Hz, 2H, (CH$_3$)$_2$C*H*N), 2.80 (s, 6H, CH_3), 0.47 (d, *J* = 6.2 Hz, 6H, CH_3), 0.01 (d, *J* = 6.2Hz, 6H, CH_3). ^{13}C{^{1}H} NMR (151 MHz, $CDCl_3$) δ: 170.6, 167.2, 151.6, 147.6, 145.5, 142.7, 136.2, 133.6, 125.9, 124.6, 123.2, 122.5, 118.0, 117.7, 47.0, 40.6, 24.2, 24.0. UV-vis (THF): λ/nm (ε/M^{-1} cm^{-1}) 334(48000), 427(19000), 517(10000), 595(sh)(2000).

X-ray Crystallography Details: Single crystals were grown by vapor diffusion of pentane vapor into concentrated THF or dichloromethane solutions. Crystals were mounted on a Bruker Apex II three-circle diffractometer using MoKa radiation (λ=0.71073 Å). The data was collected at 123(2) K and was processed and refined within the APEXII software. Structures were solved by direct methods in SHELXS and refined by standard difference Fourier techniques in the program SHELXL.[59] Hydrogen atoms were placed in calculated positions using the standard riding model and refined isotropically; all non-hydrogen atoms were refined anisotropically.

Conflicts of interest

There are no conflicts to declare.

Acknowledgements

The authors acknowledge the National Science Foundation (CHE-1846831) and the Welch Foundation (grant no. E-1887) for funding this research. Y. W. thanks the Eby Nell McElrath postdoctoral fellowship for support. B.-L. N. acknowledges the University of Houston for an undergraduate research fellowship through the SURF program.

Notes and references

1 C. K. Prier, D. A. Rankic and D. W. C. MacMillan, Visible light photoredox catalysis with transition metal complexes: Applications in organic synthesis, *Chem. Rev.*, 2013, **113**, 5322–5363.

2 Z. Zuo, D. T. Ahneman, L. Chu, J. A. Terrett, A. G. Doyle and D. W. C. MacMillan, Merging photoredox with nickel catalysis: Coupling of -carboxyl sp3-carbons with aryl halides, *Science*, 2014, **345**, 437–440.

3 T. P. Yoon, M. A. Ischay and J. Du, Visible light photocatalysis as a greener approach to photochemical synthesis, *Nat. Chem.*, 2010, **2**, 527–532.

4 Q. Zhao, F. Li, S. Liu, M. Yu, Z. Liu, T. Yi and C. Huang, Highly selective phosphorescent chemosensor for fluoride based on an iridium(III) complex containing arylborane units, *Inorg. Chem.*, 2008, **47**, 9256–9264.

5 Q. Zhao, F. Li and C. Huang, Phosphorescent chemosensors based on heavy-metal complexes, *Chem. Soc. Rev.*, 2010, **39**, 3007–3030.

6 H. (Hartmut) Yersin, *Highly efficient OLEDs with phosphorescent materials*, Weinheim : Wiley-VCH, 2008.

7 S. Lamansky, P. Djurovich, D. Murphy, F. Abdel-Razzaq, H.-E. Lee, C. Adachi, P. E. Burrows, S. R. Forrest and M. E. Thompson, Highly phosphorescent bis-cyclometalated iridium complexes: Synthesis, photophysical characterization, and use in organic light emitting diodes, *J. Am. Chem. Soc.*, 2001, **123**, 4304–4312.

8 M. S. Lowry and S. Bernhard, Synthetically tailored excited states: Phosphorescent, cyclometalated iridium(III) complexes and their applications, *Chem. – Eur. J.*, 2006, **12**, 7970–7977.

9 M. Sarma, W.-L. Tsai, W.-K. Lee, Y. Chi, C.-C. Wu, S.-H. Liu, P.-T. Chou and K.-T. Wong, Anomalously long-lasting blue PhOLED featuring phenyl-pyrimidine cyclometalated iridium emitter, *Chem*, 2017, **3**, 461–476.

10 R. D. Costa, E. Ortí, H. J. Bolink, F. Monti, G. Accorsi and N. Armaroli, Luminescent ionic transition-metal complexes for light-emitting electrochemical cells, *Angew. Chem. Int. Ed.*, 2012, **51**, 8178–8211.

11 T.-B. Gao, J.-J. Zhang, R.-Q. Yan, D.-K. Cao, D. Jiang and D. Ye, Aggregation-induced electrochemiluminescence from a cyclometalated iridium(III) complex, *Inorg. Chem.*, 2018, **57**, 4310–4316.

12 K. Dedeian, P. I. Djurovich, F. O. Garces, G. Carlson and R. J. Watts, A new synthetic route to the preparation of a series of strong photoreducing agents: fac-tris-ortho-metalated complexes of iridium(III) with substituted 2-phenylpyridines, *Inorg. Chem.*, 1991, **30**, 1685–1687.

13 A. B. Tamayo, B. D. Alleyne, P. I. Djurovich, S. Lamansky, I. Tsyba, N. N. Ho, R. Bau and M. E. Thompson, Synthesis and characterization of facial and meridional tris-cyclometalated iridium(III) complexes, *J. Am. Chem. Soc.*, 2003, **125**, 7377–7387.

14 Y. You and S. Y. Park, Inter-ligand energy transfer and related emission change in the cyclometalated heteroleptic iridium complex: Facile and efficient color tuning over the whole visible range by the ancillary ligand structure, *J. Am. Chem. Soc.*, 2005, **127**, 12438–12439.

15 C.-J. Chang, C.-H. Yang, K. Chen, Y. Chi, C.-F. Shu, M.-L. Ho, Y.-S. Yeh and P.-T. Chou, Color tuning associated with heteroleptic cyclometalated Ir(III) complexes: influence of the ancillary ligand, *Dalton Trans.*, 2007, 1881–1890.

16 J. Li, P. I. Djurovich, B. D. Alleyne, M. Yousufuddin, N. N. Ho, J. C. Thomas, J. C. Peters, R. Bau and M. E. Thompson, Synthetic control of excited-state properties in cyclometalated Ir(III) complexes using ancillary ligands, *Inorg. Chem.*, 2005, **44**, 1713–1727.

17 Y. K. Radwan, A. Maity and T. S. Teets, Manipulating the excited states of cyclometalated iridium complexes with β-ketoiminate and β-diketiminate ligands, *Inorg. Chem.*, 2015, **54**, 7122–7131.

18 Md. K. Nazeeruddin, R. Humphry-Baker, D. Berner, S. Rivier, L. Zuppiroli and M. Graetzel, Highly phosphorescence iridium complexes and their application in organic light-emitting devices, *J. Am. Chem. Soc.*, 2003, **125**, 8790–8797.

19 T. Sajoto, P. I. Djurovich, A. B. Tamayo, J. Oxgaard, W. A. Goddard and M. E. Thompson, Temperature dependence of blue phosphorescent cyclometalated Ir(III) complexes, *J. Am. Chem. Soc.*, 2009, **131**, 9813–9822.

20 C.-H. Yang, M. Mauro, F. Polo, S. Watanabe, I. Muenster, R. Fröhlich and L. De Cola, Deep-blue-emitting heteroleptic iridium(III) complexes suited for highly efficient phosphorescent OLEDs, *Chem. Mater.*, 2012, **24**, 3684–3695.

21 N. M. Shavaleev, F. Monti, R. D. Costa, R. Scopelliti, H. J. Bolink, E. Ortí, G. Accorsi, N. Armaroli, E. Baranoff, M. Grätzel and M. K. Nazeeruddin, Bright blue phosphorescence from cationic bis-cyclometalated iridium(III) isocyanide complexes, *Inorg. Chem.*, 2012, **51**, 2263–2271.

22 S. Haneder, E. D. Como, J. Feldmann, J. M. Lupton, C. Lennartz, P. Erk, E. Fuchs, O. Molt, I. Münster, C. Schildknecht and G. Wagenblast, Controlling the radiative rate of deep-blue electrophosphorescent organometallic complexes by singlet-triplet gap engineering, *Adv. Mater.*, 2008, **20**, 3325–3330.

23 H. Xiang, J. Cheng, X. Ma, X. Zhou and J. J. Chruma, Near-infrared phosphorescence: materials and applications, *Chem. Soc. Rev.*, 2013, **42**, 6128–6185.

24 C.-L. Ho, H. Li and W.-Y. Wong, Red to near-infrared organometallic phosphorescent dyes for OLED applications, *J. Organomet. Chem.*, 2014, **751**, 261–285.

25 Y.-J. Pu, R. E. Harding, S. G. Stevenson, E. B. Namdas, C. Tedeschi, J. P. J. Markham, R. J. Rummings, P. L. Burn and I. D. W. Samuel, Solution processable phosphorescent rhenium(i) dendrimers, *J. Mater. Chem.*, 2007, **17**, 4255–4264.

26 T. G. Gray, C. M. Rudzinski, D. G. Nocera and R. H. Holm, Highly emissive hexanuclear rhenium(III) clusters containing the cubic cores $[Re_6S_8]^{2+}$ and $[Re_6Se_8]^{2+}$, *Inorg. Chem.*, 1999, **38**, 5932–5933.

27 Y.-L. Tung, S.-W. Lee, Y. Chi, L.-S. Chen, C.-F. Shu, F.-I. Wu, A. J. Carty, P.-T. Chou, S.-M. Peng and G.-H. Lee, Organic light-emitting diodes based on charge-neutral RuII phosphorescent emitters, *Adv. Mater.*, 2005, **17**, 1059–1064.

28 Y. Wang, S. Liu, M. R. Pinto, D. M. Dattelbaum, J. R. Schoonover and K. S. Schanze, Excited-state structure and delocalization in ruthenium(II)−bipyridine complexes that contain phenyleneethynylene substituents, *J. Phys. Chem. A*, 2001, **105**, 11118–11127.

29 B. Carlson, G. D. Phelan, W. Kaminsky, L. Dalton, X. Jiang, S. Liu and A. K.-Y. Jen, Divalent osmium complexes: synthesis, characterization, strong red phosphorescence, and electrophosphorescence, *J. Am. Chem. Soc.*, 2002, **124**, 14162–14172.

30 Y.-L. Tung, P.-C. Wu, C.-S. Liu, Y. Chi, J.-K. Yu, Y.-H. Hu, P.-T. Chou, S.-M. Peng, G.-H. Lee, Y. Tao, A. J. Carty, C.-F. Shu and F.-I. Wu, Highly efficient red phosphorescent osmium(II) complexes for OLED applications, *Organometallics*, 2004, **23**, 3745–3748.

31 H. Fukagawa, T. Shimizu, H. Hanashima, Y. Osada, M. Suzuki and H. Fujikake, Highly efficient and stable red phosphorescent organic light-emitting diodes using platinum complexes, *Adv. Mater.*, 2012, **24**, 5099–5103.
32 P. Mandapati, J. D. Braun, C. Killeen, R. L. Davis, J. A. G. Williams and D. E. Herbert, Luminescent platinum(II) complexes of *N ^N^N* amido ligands with benzannulated *N*-heterocyclic donor arms: Quinolines offer unexpectedly deeper red phosphorescence than phenanthridines, *Inorg. Chem.*, 2019, **58**, 14808–14817.
33 X. Yang, X. Xu, J. Zhao, J. Dang, Z. Huang, X. Yan, G. Zhou and D. Wang, Phosphorescent platinum(II) complexes bearing 2-vinylpyridine-type ligands: Synthesis, electrochemical and photophysical properties, and tuning of electrophosphorescent behavior by main-group moieties, *Inorg. Chem.*, 2014, **53**, 12986–13000.
34 E. Rossi, L. Murphy, P. L. Brothwood, A. Colombo, C. Dragonetti, D. Roberto, R. Ugo, M. Cocchi and J. A. G. Williams, Cyclometallated platinum(ii) complexes of 1,3-di(2-pyridyl)benzenes: tuning excimer emission from red to near-infrared for NIR-OLEDs, *J. Mater. Chem.*, 2011, **21**, 15501.
35 S. M. Borisov, G. Nuss, W. Haas, R. Saf, M. Schmuck and I. Klimant, New NIR-emitting complexes of platinum(II) and palladium(II) with fluorinated benzoporphyrins, *J. Photochem. Photobiol. Chem.*, 2009, **201**, 128–135.
36 M. Cocchi, D. Virgili, V. Fattori, J. A. G. Williams and J. Kalinowski, Highly efficient near-infrared organic excimer electrophosphorescent diodes, *Appl. Phys. Lett.*, 2007, **90**, 023506.
37 M. Z. Shafikov, R. Daniels, P. Pander, F. B. Dias, J. A. G. Williams and V. N. Kozhevnikov, Dinuclear design of a Pt(II) complex affording highly efficient red emission: Photophysical properties and application in solution-processible OLEDs, *ACS Appl. Mater. Interfaces*, 2019, **11**, 8182–8193.
38 G. Cheng, Q. Wan, W. Ang, C. Kwong, W. To, P. Chow, C. Kwok and C. Che, High-performance deep-red/near-infrared OLEDs with tetradentate [Pt(O^N^C^N)] emitters, *Adv. Opt. Mater.*, 2019, **7**, 1801452.
39 M. Bixon and J. Jortner, Intramolecular radiationless transitions, *J. Chem. Phys.*, 1968, **48**, 715–726.
40 R. Englman and J. Jortner, The energy gap law for radiationless transitions in large molecules, *Mol. Phys.*, 1970, **18**, 145–164.
41 S. D. Cummings and R. Eisenberg, Tuning the excited-state properties of platinum(II) diimine dithiolate complexes, *J. Am. Chem. Soc.*, 1996, **118**, 1949–1960.
42 P.-N. Lai, C. H. Brysacz, M. K. Alam, N. A. Ayoub, T. G. Gray, J. Bao and T. S. Teets, Highly efficient red-emitting bis-cyclometalated iridium complexes, *J. Am. Chem. Soc.*, 2018, **140**, 10198–10207.
43 P.-N. Lai and T. S. Teets, Ancillary ligand effects on red-emitting cyclometalated iridium complexes, *Chem. – Eur. J.*, 2019, **25**, 6026–6037.
44 J.-H. Shon and T. S. Teets, Potent bis-cyclometalated iridium photoreductants with β-diketiminate ancillary ligands, *Inorg. Chem.*, 2017, **56**, 15295–15303.
45 J.-H. Shon, S. Sittel and T. S. Teets, Synthesis and characterization of strong cyclometalated iridium photoreductants for application in photocatalytic aryl bromide hydrodebromination, *ACS Catal.*, 2019, **9**, 8646–8658.
46 Y. Liu, K. Ye, Y. Fan, W. Song, Y. Wang and Z. Hou, Amidinate-ligated iridium(III) bis(2-pyridyl)phenyl complex as an excellent phosphorescent material for electroluminescence devices, *Chem. Commun.*, 2009, 3699–3701.
47 Z.-T. Yu, Y.-J. Yuan, J.-G. Cai and Z.-G. Zou, Charge-neutral amidinate-containing iridium complexes capable of efficient photocatalytic water reduction, *Chem. - Eur. J.*, 2013, **19**, 1303–1310.
48 V. K. Rai, M. Nishiura, M. Takimoto and Z. Hou, Substituent effect on the electroluminescence efficiency of amidinate-ligated bis(pyridylphenyl) iridium(III) complexes, *J. Mater. Chem. C*, 2014, **2**, 5317–5326.
49 E. Zysman-Colman, Ed., *Iridium(III) in Optoelectronic and Photonics Applications*, John Wiley & Sons, Inc, Chichester, West Sussex, 2017.
50 R. A. Maya, A. Maity and T. S. Teets, Fluorination of cyclometalated iridium β-ketoiminate and β-diketiminate complexes: Extreme redox tuning and ligand-centered excited states, *Organometallics*, 2016, **35**, 2890–2899.
51 H.-C. Li, P.-T. Chou, Y.-H. Hu, Y.-M. Cheng and R.-S. Liu, Synthesis, characterization, and photophysical properties of iridium complexes with an 8-phenylquinoline framework. The first six-membered chelated iridium complexes for electroluminance, *Organometallics*, 2005, **24**, 1329–1335.
52 J. M. Fernandez-Hernandez, E. Longhi, R. Cysewski, F. Polo, H.-P. Josel and L. De Cola, Photophysics and electrochemiluminescence of bright cyclometalated Ir(III) complexes in aqueous solutions, *Anal. Chem.*, 2016, **88**, 4174–4178.
53 C. You, D. Liu, F. Meng, Y. Wang, J. Yu, S. Wang, S. Su and W. Zhu, Iridium(III) phosphors with rigid fused-heterocyclic chelating architectures for efficient deep-red/near-infrared emissions in polymer light-emitting diodes, *J. Mater. Chem. C*, 2019, **7**, 10961–10971.
54 H. U. Kim, H. J. Jang, W. Choi, M. Kim, S. Park, T. Park, J. Y. Lee and B. K. S., Ancillary ligand-assisted robust deep-red emission in iridium(III) complexes for solution-processable phosphorescent OLEDs, *J. Mater. Chem. C*, 2019, **7**, 4143–4154.
55 A. J. Lees, The luminescence rigidochromic effect exhibited by organometallic complexes: Rationale and applications, *Comments Inorg. Chem.*, 1995, **17**, 319–346.
56 A. B. Pangborn, M. A. Giardello, R. H. Grubbs, R. K. Rosen and F. J. Timmers, Safe and convenient procedure for solvent purification, *Organometallics*, 1996, **15**, 1518–1520.
57 M. Nonoyama, Benzo[h]quinolin-10-yl-N iridium(III) complexes, *Bull. Chem. Soc. Jpn.*, 1974, **47**, 767–768.
58 P. G. Seybold and M. Gouterman, Porphyrins: XIII: Fluorescence spectra and quantum yields, *J. Mol. Spectrosc.*, 1969, **31**, 1–13.
59 G. M. Sheldrick, A short history of *SHELX*, *Acta Crystallogr. A*, 2008, **64**, 112–122.